Monitoring landslides and tectonic motions with the Permanent Scatterers Technique

Carlo Colesanti [a,b,1], Alessandro Ferretti [a,b,*,1], Claudio Prati [a,b], Fabio Rocca [a,b]

[a]*Dipartimento di Elettronica e Informazione, Politecnico di Milano, Piazza Leonardo da Vinci, 32-20133 Milan, Italy*
[b]*Tele-Rilevamento Europa-T.R.E. S.r.l., Piazza Leonardo da Vinci, 32-20133 Milan, Italy*

Abstract

Spaceborne differential synthetic aperture radar interferometry (DInSAR) has already proven its potential for mapping ground deformation phenomena, e.g. volcano dynamics. However, atmospheric disturbances as well as phase decorrelation have prevented hitherto this technique from achieving full operational capability. These drawbacks are overcome by carrying out measurements on a subset of image pixels corresponding to pointwise stable reflectors (Permanent Scatterers, PS) and exploiting long temporal series of interferometric data.

Results obtained by processing 55 images acquired by the European Space Agency (ESA) ERS SAR sensors over Southern California show that the PS approach pushes measurement accuracy very close to its theoretical limit (about 1 mm), allowing the description of millimetric deformation phenomena occurring in a complex fault system. A comparison with corresponding displacement time series relative to permanent GPS stations of the Southern California Integrated GPS network (SCIGN) is carried out. Moreover, the pixel-by-pixel character of the PS analysis allows the exploitation of individual phase stable radar targets in low-coherence areas. This makes spaceborne interferometric measurements possible in vegetated areas, as long as a sufficient spatial density of individual isolated man-made structures or exposed rocks is available.

The evolution of the Ancona landslide (central Italy) was analysed by processing 61 ERS images acquired in the time span between June 1992 and December 2000. The results have been compared with deformation values detected during optical levelling campaigns ordered by the Municipality of Ancona.

The characteristics of PS, GPS and optical levelling surveying are to some extent complementary: a synergistic use of the three techniques could strongly enhance quality and reliability of ground deformation monitoring.
© 2002 Elsevier Science B.V. All rights reserved.

Keywords: Permanent Scatterers Technique; Synthetic aperture radar interferometry; Landslides; Tectonics; Monitoring

1. Introduction

The interferometric approach is based on the phase comparison of synthetic aperture radar (SAR) images, gathered at different times with slightly different looking angles (Gabriel et al., 1989; Massonnet and Feigl, 1998; Rosen et al., 2000; Bamler and Hartl, 1998). Theoretically, it has the potential to detect millimetric

---

* Corresponding author. Dipartimento di Elettronica e Informazione, Politecnico di Milano, Piazza Leonardo da Vinci, 32-20133 Milan, Italy. Tel.: +39-22-3993451; fax: +39-22-3993413.

E-mail addresses: aferrett@elet.polimi.it, alessandro.ferretti@treuropa.com (A. Ferretti).

[1] Tel.: + 39-22-3993451; fax: + 39-22-3993413.

target motion phenomena along the sensor-target (Line-of-Sight, LOS) direction. In particular, significant results have been obtained in mapping volcano dynamics (Massonnet et al., 1995), coseismic (Massonnet et al., 1993; Peltzer et al., 1999) and post-seismic (Massonnet et al., 1994; Peltzer et al., 1996; Massonnet et al., 1996) deformation along active seismic faults, as well as slope instability and failure (Fruneau et al., 1995) phenomena. Apart from cycle ambiguity problems, limitations are mainly due to temporal and geometrical decorrelation (Zebker and Villasenor, 1992), as well as to atmospheric artifacts (Massonnet and Feigl, 1995; Hanssen, 1998; Williams et al., 1998; Goldstein, 1995; Zebker et al., 1997).

Temporal decorrelation makes interferometric measurements unfeasible where the electromagnetic profiles and/or the positions of the scatterers change with time within the resolution cell. The use of short revisiting times is not a solution, since slow terrain motion (e.g. creeping) cannot be detected. Reflectivity variations as a function of the incidence angle are usually referred to as geometrical decorrelation and further limit the number of image pairs suitable for interferometric applications, unless this phenomenon is reduced due to the pointwise character of the target (e.g. a corner reflector). In areas affected by either kind of decorrelation, reflectivity phase contributions are no longer compensated by generating the interferogram (Zebker and Villasenor, 1992), and phase terms due to possible target motion cannot be highlighted (Massonnet and Feigl, 1998). Finally, atmospheric heterogeneity superimposes on each SAR acquisition an atmospheric phase screen (APS) that can seriously compromise accurate deformation monitoring (Massonnet and Feigl, 1995, 1998). Indeed, even considering areas slightly affected by decorrelation, it may be extremely difficult to discriminate displacement phase contributions from the atmospheric signature, at least using individual interferograms (Massonnet and Feigl, 1995, 1998; Sandwell and Price, 1998).

2. The Permanent Scatterers Technique

Atmospheric artifacts show a strong spatial correlation within each individual SAR acquisition (Hanssen, 1998; Williams et al., 1998; Goldstein, 1995), but are uncorrelated in time. Conversely, target motion is usu-

ally strongly correlated in time and can exhibit different degrees of spatial correlation depending on the particular displacement phenomenon at hand (e.g. subsidence due to exploitation of ground water resources (Ferretti et al., 2000) or oil/gas extraction, deformation along seismic faults, localised sliding areas, collapsing buildings).

Atmospheric effects can then be estimated and removed by combining data from long time series of SAR images (Ferretti et al., 2000, 2001), as those in the European Space Agency (ESA) ERS archive, gathering data since late 1991. In order to exploit all the available images and improve the accuracy of APS estimation, only scatterers slightly affected by both temporal and geometrical decorrelation should be selected (Ferretti et al., 2000, 2001). Phase stable pointwise targets, hereafter called Permanent Scatterers (PS), can be detected on the basis of a statistical analysis on the amplitudes of their electromagnetic returns (Ferretti et al., 2001).

All available images are focused and co-registered on the reference sampling grid of a unique master acquisition (Basilico, 2000), which should be selected keeping as low as possible the dispersion of the normal baseline values. Radiometric correction is carried out through power normalisation in order to make comparable the amplitude returns relative to different acquisitions. Amplitude data are analysed on a pixel-by-pixel basis (i.e. without spatial averaging) computing the so-called amplitude stability index (Ferretti et al., 2000, 2001), ratio between the average amplitude return relative to each individual pixel and its standard deviation. This statistical quantity provides precious information about the expected phase stability of the scattering barycentre of each sampling cell (Ferretti et al., 2001). Simple thresholding (e.g. with a value of $2.5-3$) on the amplitude stability index allows the identification of a sparse grid of Permanent Scatterers Candidates (PSC), points that are expected having a PS behaviour (Ferretti et al., 2001).

PSC are actually a small subset of the PS as a whole since the phase stability of many PS cannot be inferred directly from the amplitude stability index (Ferretti et al., 2001). As explained in the forthcoming paragraphs, their spatial density is usually sufficient ($\geq 3-4$ PS/km^2) to carry out the reconstruction and compensation of the APS.

Exploiting jointly all available Tandem pairs (i.e. ERS-1/2 data with a temporal baseline of 1 day), a

conventional InSAR Digital Elevation Model (DEM) can be reconstructed (Ferretti et al., 1999). As an alternative, an already available DEM (e.g. photogrammetric) can be resampled on the master image grid.

Given $N+1$ ERS-SAR data, N differential interferograms can be generated with respect to the common master acquisition. Since Permanent Scatterers are not affected by decorrelation, all interferograms, regardless of their normal and temporal baseline, can be involved in the PS processing.

The phase (of each single pixel) of interferogram i is:

$$\phi_i = \frac{4\pi}{\lambda} r_{Ti} + \alpha_i + n_i + \phi_{topo-res} \qquad (1)$$

where $\lambda = 5.66$ cm, r_{Ti} is the target motion (with respect to its position at the time of the master acquisition) possibly occurring, α_i is the atmospheric phase contribution (referred to the master image APS), n_i is the decorrelation noise, and $\phi_{topo-res}$ is the residual topographic phase contribution due to inaccuracy in the reference DEM.

The goal of the PS approach is the separation of these phase terms. The basic idea is to work on the PSC grid, computing in each interferogram i the phase difference $\Delta\phi_i$, relative to pairs of PSC within a certain maximum distance (e.g. 2–3 km).

In fact, since APS is strongly correlated in space, the differential atmospheric phase contributions relative to close PSC will be extremely low (for points less than 1 km apart $\sigma_{\Delta\alpha^2}$ is usually lower than 0.1 rad^2 (Williams et al., 1998)). The phase difference relative to close PSC is, therefore, only slightly affected by APS. Moreover, if both PSC effectively exhibit PS behaviour (i.e. are not affected by decorrelation), n_i and, consequently, Δn_i will show a very low variance as well.

Assuming the target motion is uniform in time (i. e. constant rate deformation), the first term in (Eq. (1)) can be written as $(4\pi/\lambda)vT_i$, where v is the average deformation rate along the ERS Line-of-Sight (LOS) and T_i is the temporal baseline with respect to the master acquisition.

For a couple of PSC (1, 2), the phase difference in each interferogram i is:

$$\Delta\phi_{1,2,i} = \frac{4\pi}{\lambda} \Delta v_{1,2} T_i + K_\varepsilon \Delta\varepsilon_{1,2} B_{n,i} + w_{1,2,i} \qquad (2)$$

where $\Delta v_{1,2}$ and $\Delta\varepsilon_{1,2}$ are the differential LOS velocity and the differential DEM inaccuracy relative to the

PS couple at hand. $B_{n,i}$ is the normal baseline of the interferogram i (with respect to the master image). Finally, $w_{1,2,i}$ is the residual phase term, gathering all other contributions, namely decorrelation noise Δn_i, differential APS $\Delta\alpha_i$, and possible time nonuniform deformation.
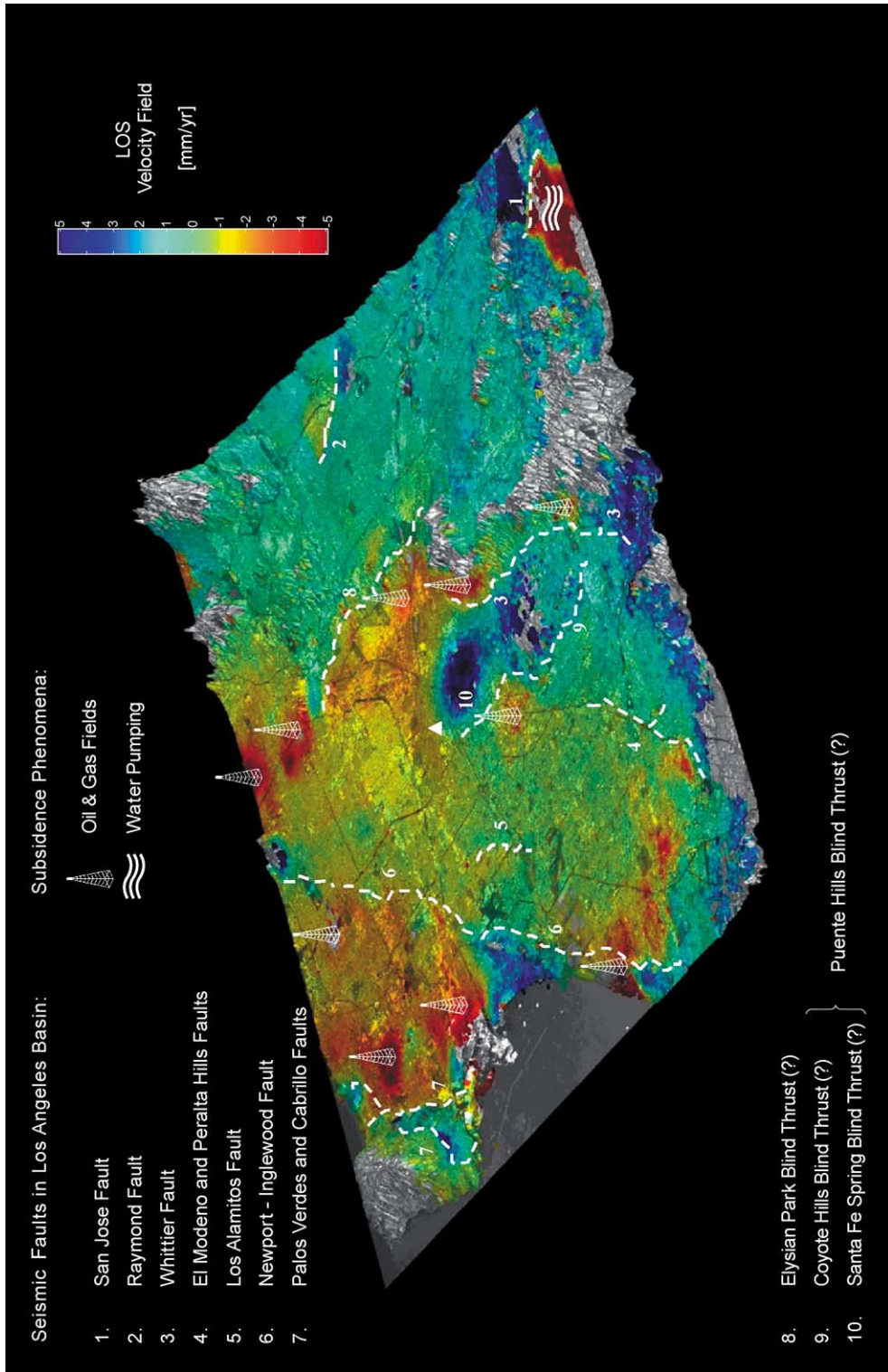
Since N differential interferograms are available for each couple of PSC, there are N equations in the unknowns $\Delta v_{1,2}$ and $\Delta\varepsilon_{1,2}$. Unfortunately, the phase values $\Delta\phi_{1,2,i}$ are wrapped, and, therefore, the system is nonlinear. In fact, even if no deformation is occurring, the differential residual topographic phase $\Delta\phi_{topo-res,1,2,i}$ will often exceed one phase cycle in large baseline interferograms (e.g. for a 1200 m baseline interferogram the ambiguity height (Rosen et al., 2000; Ferretti et al., 1999) is around 7.5 m, i.e. a differential error of 7.5 m in the DEM values relative to the PSC (1,2) would introduce a complete phase cycle).

The task can be thought of as a spectral estimation problem and the unknowns are estimated jointly in a maximum likelihood (ML) sense as the position ($\Delta v_{1,2}$, $\Delta\varepsilon_{1,2}$) of the peak in the periodogram of the complex signal $e^{j\Delta\phi(1,2,i)}$, which is available on an irregular sampling grid along both dimensions temporal and normal baseline, T_i and $B_{n,i}$. Of course, this is feasible only as long as the residual phase terms $w_{1,2,i}$ are low enough (a reasonable figure could be $\sigma(w_{1,2}) \leq 0.6$ [rad]), i.e. as long as the two PSC involved in the equation set at hand effectively exhibit a PS behaviour (low decorrelation noise), are not affected by differential time nonuniform deformation and are close enough to keep low the differential APS term as well (to meet this last condition, the PSC grid should be dense enough, e.g. at least 3–4 PS/km^2, as previously mentioned).

As soon as $\Delta v_{1,2}$ and $\Delta\varepsilon_{1,2}$ have been estimated, the phase differences $\Delta\phi_i$ can be unwrapped correctly (obviously assuming $|w_{1,2,i}| < \pi$). Integrating the unwrapped phase differences relative to every couple of PSC, each interferogram can be unwrapped in correspondence of the sparse grid of PSC. $\Delta v_{1,2}$ and $\Delta\varepsilon_{1,2}$ can be integrated as well (assuming $v = v_0$ and $\varepsilon = \varepsilon_0$ for a reference point), obtaining v and ε.

The unwrapped atmospheric phase contribution relative to each PSC can then be obtained as the difference:

$$[\alpha_i]_{uw} = [\phi_i]_{uw} - \frac{4\pi}{\lambda} vT_i - K_\varepsilon \varepsilon B_{n,i} \qquad (3)$$

Seismic Faults in Los Angeles Basin:

1. San Jose Fault
2. Raymond Fault
3. Whittier Fault
4. El Modeno and Peralta Hills Faults
5. Los Alamitos Fault
6. Newport - Inglewood Fault
7. Palos Verdes and Cabrillo Faults

8. Elysian Park Blind Thrust (?)
9. Coyote Hills Blind Thrust (?)
10. Santa Fe Spring Blind Thrust (?)

Puente Hills Blind Thrust (?)

Subsidence Phenomena:

Oil & Gas Fields

Water Pumping

LOS
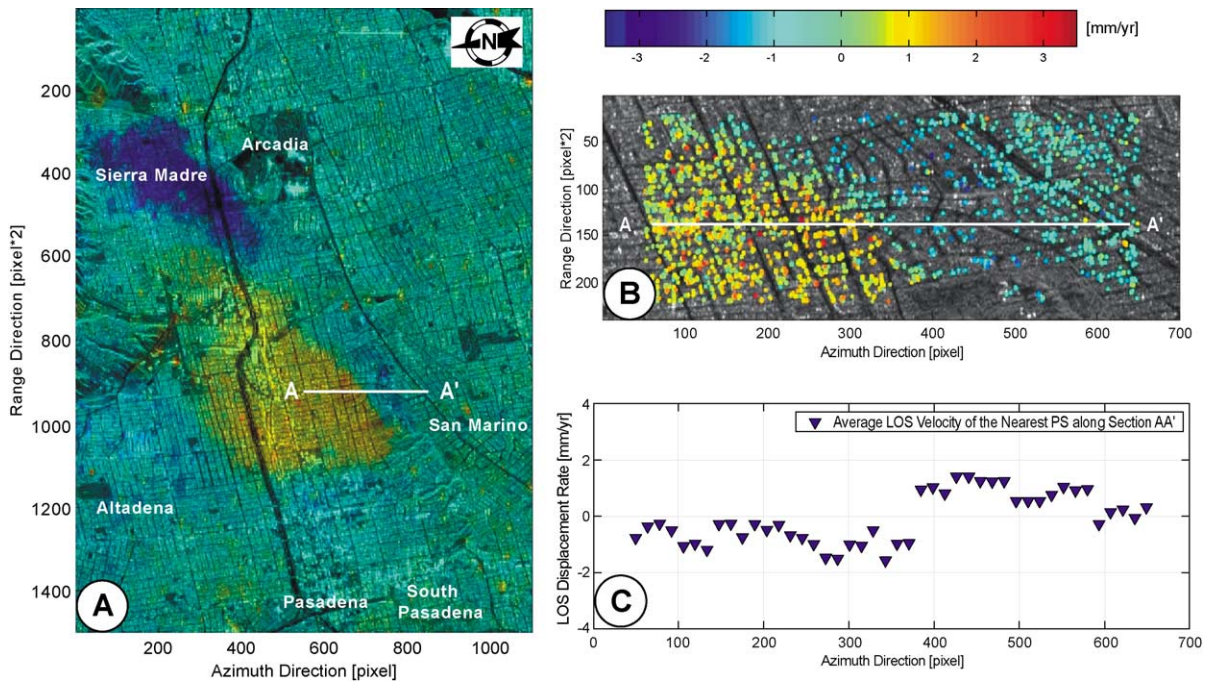Velocity Field
[mm/yr]

5
4
3
2
1
0
-1
-2
-3
-4
-5

Fig. 2. (A) Estimated LOS velocity field across the Raymond fault. In order to minimise interpolation artifacts, data are reported in SAR coordinates (range, azimuth) rather than in geographical coordinates. The sampling step is about 4 m both in slant range and azimuth (ERS images have been interpolated by a factor of 2 in range direction). PS density is very high (over 200 PS/km^2), so that the estimated LOS velocity field looks continuous. As in Fig. 1, velocity values are computed with respect to the reference point in Downey (SCIGN, 2000) assumed motionless. (B) Close up on cross section AA′. Location and velocity of the PS have been highlighted and their density can be better appreciated. The relative dispersion of the velocity values in the two areas separated by the fault is lower than 0.4 mm/year. (C) LOS displacement rates relative to the PS along section AA′. The stepwise discontinuity of about 2 mm/year in the average deformation rate can be identified easily and the hanging wall of the fault can be located with a spatial resolution of a few tens of meters.

Of course, possible time nonuniform deformation phenomena are, so far, wrongly interpreted as atmospheric artifacts. The two phase contributions exhibit, however, a different behaviour in time: APS is uncorrelated whereas nonlinear motion (NLM) is usually strongly correlated.

Assuming a time decaying exponential correlation for NLM, corrected with a 1-year periodic term for

---

Fig. 1. Perspective view of the estimated velocity field in the direction of the ERS satellites Line-of-Sight, on an area ca. 60×60 km^2 in the Los Angeles basin. The system sensitivity to target displacements is expressed by the unitary vector (Massonnet et al., 1996): $e = 0.41$; $n = -0.09$; $u = 0.91$ (east, north, up) relative to the reference point chosen in Downey, (SCIGN, 2000) approximately in the centre of the test site. Thus, interferometric sensitivity is maximum for vertical displacements. The reference digital elevation model was estimated directly from SAR data (Ferretti et al., 1999) and no a priori information was used with exception of the coordinates of one Ground Control Point. Topographic relief has been exaggerated for visualisation. The velocity field is superimposed on the incoherent average of all the images, and values were saturated at ± 5 mm/year for visualisation purposes only. The reference point, marked in white and supposed motionless, was chosen at Downey, where a permanent GPS station (DYHS) is run since June 1998 by SCIGN (2000). Areas with low PS density are left uncoloured as well as areas affected by strong time nonuniform motion (e.g. the harbour of Long Beach (Department of Oil Properties, 2000)), since in this case, the average deformation rate is not a very significant index. Dashed lines denote known faults and suggested locations of blind thrust faults (California Department of Conservation, 1994; Oskin et al., 2000; Shaw and Shearer, 1999). Areas affected by subsidence due to water pumping (Pomona; Ferretti et al., 2000) and oil or gas withdrawal (Department of Oil Properties, 2000) can be identified immediately.

possible NLM seasonal effects, APS and time nonuniform deformation can be separated at PSC, through Wiener filtering along the temporal dimension (taking account of the irregular sampling in time, induced by missing ERS acquisitions).

Due to the high spatial correlation of APS, even a sparse grid of PSC enables the retrieval of the atmospheric components on the whole of the imaged area, provided that the PS density is larger than 3–4 PS/km^2 (Williams et al., 1998). Kriging interpolation (Wackernagel, 1998) allows at once optimum filtering (in particular removal of outliers) and resampling of APS on the regular SAR grid of ERS differential interferograms.

Even though precise state vectors are usually available for ERS satellites (Scharroo and Visser, 1998), the impact of orbit indeterminations on the interferograms cannot be neglected (Ferretti et al., 2000). Estimated APS is actually the sum of two-phase contributions: atmospheric effects and orbital terms due to inaccuracy in the sensor orbit assumed for interferometric processing (Ferretti et al., 2000). However, the latter correspond to low-order phase polynomials and do not change the low wave number character of the signal to be estimated on the sparse PSC grid.

Differential interferograms are compensated for the retrieved APS (actually APS + orbit indetermination phase term), and the same joint v, ε estimation step, previously carried out on phase differences relative to PSC couples, can now be performed working on APS corrected interferograms on a pixel-by-pixel basis, identifying all Permanent Scatterers.

Of course, for carrying out a Permanent Scatterers analysis, a sufficient number of images should be available (usually at least 25–30), in order to properly identify PSC with statistical indices and correctly estimate $\Delta v_{1,2}$ and $\Delta\varepsilon_{1,2}$.

3. Output products of a Permanent Scatterers analysis

At Permanent Scatterers, submetre elevation accuracy (due to the wide dispersion of the incidence angles available, usually ± 70 mdeg. with respect to the reference orbit) and detection of millimetric deforma-

Table 1
Comparison between GPS and PS average deformation rates along the ERS Line-of-Sight

Station ID	Location	GPS[a] (mm/year)	SAR-b[b] (mm/year)	Δ (mm/year)	SAR-μ[c] (mm/year)	SAR-σ[c] (mm/year)	N[d]
AZU1	Azusa	− 0.21	0.38	0.59	1.46	0.89	14
BRAN	Burbank	− 4.19[e]	0.39	4.58[e]	0.45	0.1	2
CIT1	Pasadena	2.12	2.01	− 0.11	1.44	0.38	48
CLAR	Claremont	6.27	4.91	− 1.36	3.52	0.77	41
HOLP	Hollydale	− 3.12	− 2.53	0.59	− 1.54	0.71	7
JPLM	Pasadena	1.49	0.6	− 0.89	0.65	0.66	49
LBCH	Long Beach	− 10.48[e]	− 2.29	8.19[e]	− 3.29	0.65	7
LEEP	Hollywood	− 0.37	0.25	0.62	− 0.09	0.50	33
LONG	Irwindale	4.58[e]	1.32	− 3.26[e]	0.31	0.51	18
USC1	Los Angeles	− 4.41	− 4.42	− 0.01	− 3.57	0.55	26
WHC1	Whittier	− 2.99	− 2.96	0.03	− 3.08	0.41	9

   [a] SCIGN GPS data processed at JPL (SCIGN, 2000; Heflin et al., 2000). The LOS projection of the common-mode regional term (− 19.3 mm/year, estimated exploiting JPL GPS solutions, provided in May 2000 (Heflin et al., 2000)) has been removed from GPS rates.

   [b] Best match among the N PS nearest to the estimated position of the GPS station. For CLAR, JPLM, LBCH and LEEP stations (SCIGN, 2000), just the nearest PS has been considered.

   [c] Mean and standard deviation of the velocity values of the N nearest PS. The dispersion value should not be confused with the precision of the PS technique since it strongly depends on the gradient of the velocity field, influenced by local deformation phenomena like motion along active faults and subsidence in correspondence of oil fields.

   [d] Number of PS identified in a 100-m ray circle around the estimated position of the GPS receiver. Due to a lower PS density, for CLAR and JPLM stations, a 500-m ray circle was used, while for LEEP, a 1500-m ray was needed.

   [e] JPL GPS solutions are not consistent with GPS rates (available on the web) estimated at these stations by the Scripps Orbit and Permanent Array Center (SOPAC) (SCIGN, 2000; SOPAC, 2000). Compensating for the LOS common mode term (− 17.9 mm/year, estimated exploiting SOPAC deformation trends, May 2000), SOPAC rates along LOS direction are: BRAN: − 0.45 mm/year; LBCH: − 2.60 mm/year; LONG: − 0.36 mm/year, and are in much better agreement with PS DInSAR results.

tion (due to the high phase coherence of PS) can be achieved, once APSs are estimated and removed (Ferretti et al., 2000, 2001). In particular, the relative target LOS velocity can be estimated with unprecedented accuracy, sometimes even better than 0.1 mm/year., exploiting the long time span on very stable PS.

Final results of the multi-interferogram Permanent Scatterers approach are (Ferretti et al., 2000, 2001):

• Map of the PS identified in the image and their coordinates: latitude, longitude and precise elevation (accuracy on elevation better than 1 m).
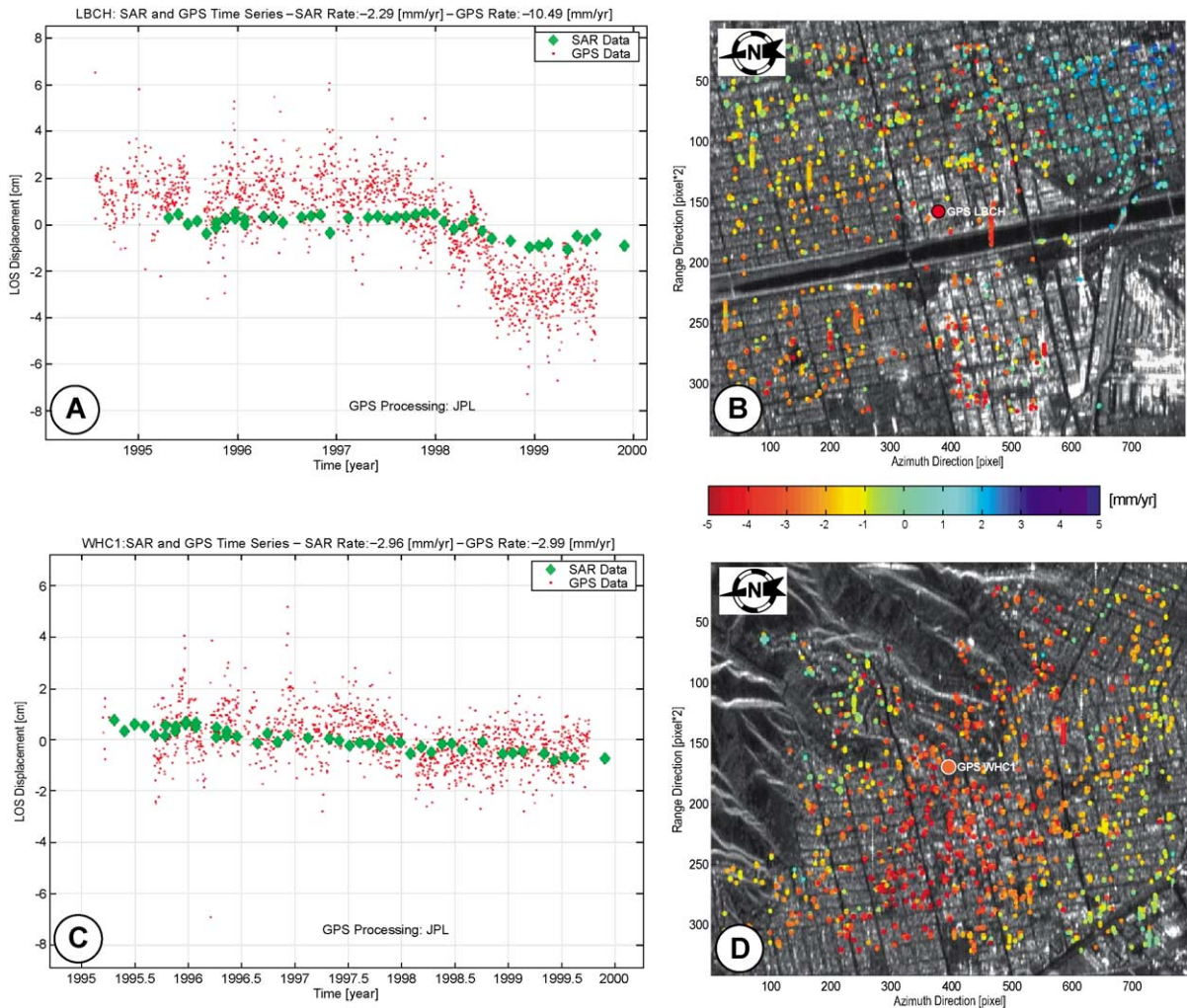

Fig. 3. (A) Comparison between JPL GPS time series (Heflin et al., 2000), relative to the SCIGN station LBCH at Long Beach (SCIGN, 2000), and the estimated displacement of the PS nearest to the GPS receiver. On this station, poor agreement between the LOS velocity values estimated by the two systems was found (see Table 1 for details). However, both time series trend similarly, showing centimetric subsidence in 1998. The different signal-to-noise ratios are mainly due to the operating frequencies of the two systems: L-band for GPS and C-band for SAR. (B) Close up on the area hosting the permanent GPS receiver LBCH and the 800 closest PS. The colour of each PS benchmark indicates its average LOS velocity (values are saturated to ± 5 mm/year for visualisation purposes only). (C) Same as in (A) for the SCIGN permanent GPS station WHC1 (SCIGN, 2000; Heflin et al., 2000), located at Whittier College. The agreement SAR-GPS is excellent. (D) Same as in (B) for the area surrounding the GPS station WHC1 (1000 PS available). Sharp subsidence phenomena in this area are due to oil extraction at the Whittier oil field (Department of Oil Properties, 2000).
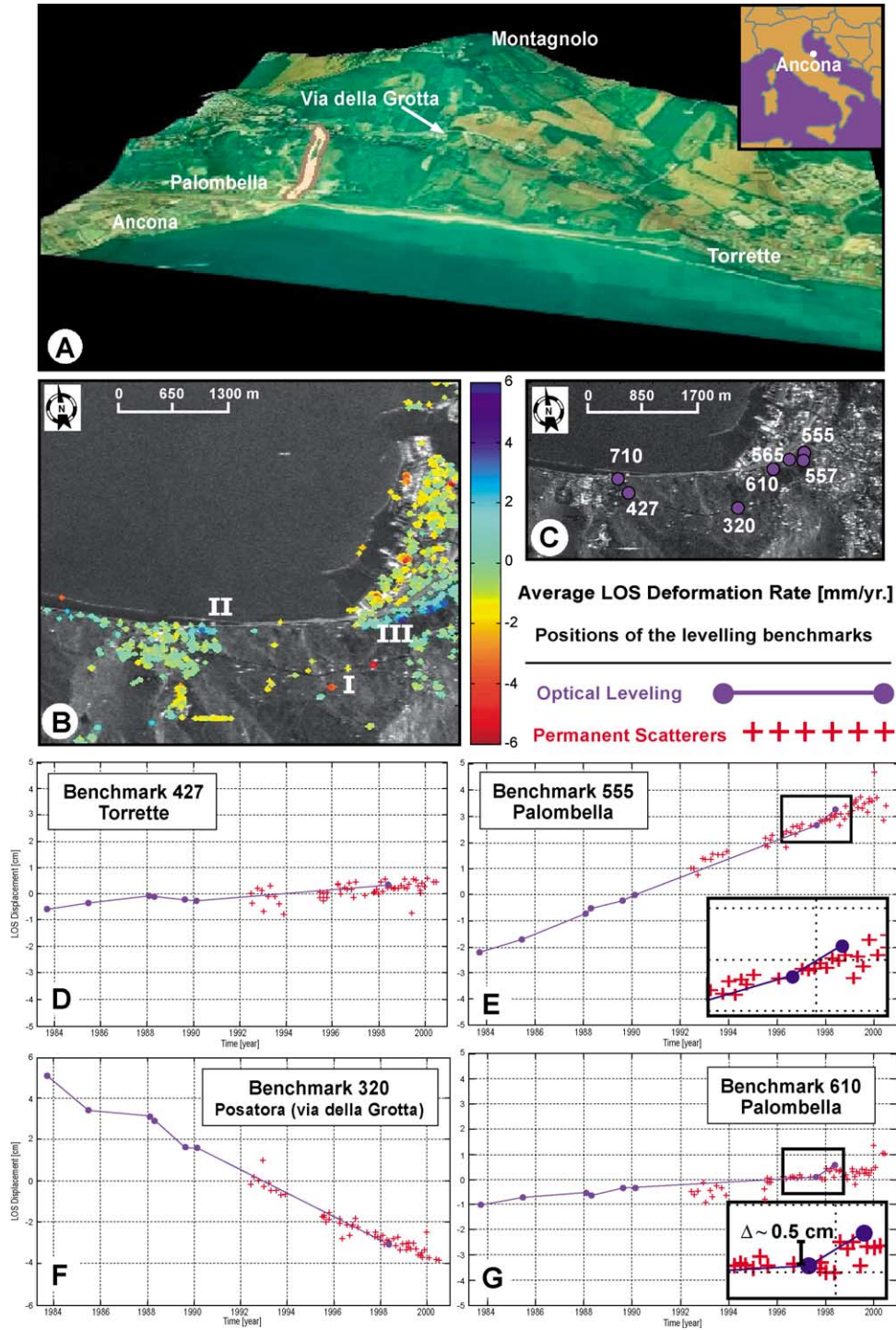
• Average LOS deformation rate of every PS (accuracy usually between 0.1 and 1 mm/year, depending on the number of available interferograms and on the phase stability of each single PS).

• Displacement time series showing the relative (i.e. with respect to a unique reference image) LOS position of PS in correspondence of each SAR acquisition. Time series represent, therefore, the LOS motion component of PS as a function of time (accuracy on single measurements usually ranging from 1 to 3 mm).

As in all differential interferometry applications, results are not absolute both in time and space. Deformation data are referred to the master image (in time) and results are computed with respect to a reference point of known elevation and motion (in space).

4. PS analysis in the Los Angeles basin: monitoring seismic faults and comparing PS and GPS data

In Fig. 1, a perspective view of the LOS velocity field estimated by exploiting 55 ERS acquisitions from 1992 to 1999 over southern California is displayed. More than 500,000 PS were identified, with an average density of 150 PS/km². The reference point, supposed motionless, was chosen at Downey

(in the centre of the test site, 20 km SE of downtown Los Angeles), referring to the data of a permanent GPS station of the Southern California Integrated GPS Network (SCIGN, 2000).

Subsidence phenomena due to oil and gas extraction (Department of Oil Properties, 2000) and water pumping (Ferretti et al., 2000) are clearly visible in the picture. Moreover, local maxima of the velocity field gradient are strongly correlated to the locations of known active seismic faults (California Department of Conservation, 1994). The position of hanging walls as well as the LOS component of the slip rate can be inferred very precisely whenever a high density of accurate measurements is available (Fig. 2).

In particular, the velocity field shows local abrupt variations that correlate well with blind thrust faults (Oskin et al., 2000; Shaw and Shearer, 1999), that is, shallow-dipping reverse faults that (i) terminate before reaching the surface, (ii) exhibit millimetric yearly slip rates and (iii) are difficult to locate and map before occurrence of coseismic displacements along them.

Identification and monitoring of blind thrusts faults in compressional tectonic settings (such as California) is a crucial challenge for reliable seismic risk assessment. The velocity field mapped in Fig. 1 shows a local

Fig. 4. (A) Aerial photograph (superimposed on a low resolution DEM) of the area affected by the "Grande Frana di Ancona" (Great Ancona Landslide), central Italy. The vertical scale for topography has been exaggerated for visualisation purposes. The slope faces north towards the sea with an average inclination of around 10° and is characterised by several successions of scarps, trenches and counter slopes (data: courtesy of the Municipality of Ancona). (B) Estimated average Line-of-Sight deformation rate of individual Permanent Scatterers in the sliding area and in its immediate surroundings (about 4×5 km²). Around 820 PS were identified, 12 in the descent front area (I) , mainly along "via della Grotta". Several tens of Permanent Scatterers are available on both sides of the urbanised ascent front area (respectively in Torrette (II) and Palombella (III)). The system sensitivity to target displacements is expressed by the unitary vector (Massonnet et al., 1996): $e = 0.37$; $n = -0.09$; $u = 0.92$ (east, north, up) relative to the harbour (less than 3 km apart from the descent front of the landslide). All velocity values are computed with respect to a reference point, located between Chiaravalle and Camerata Picena, approximately 11 km SW of Ancona and assumed motionless. No a priori information was used with exception of the coordinates of one Ground Control Point. Position and LOS deformation rate of each PS are identified by a coloured marker superimposed on the multi-image reflectivity map, displayed in SAR coordinates, range and azimuth. Since data were not geocoded, the horizontal scale is given as a qualitative reference. Displacement rates were saturated at ± 6 mm/ year for visualisation purposes. In the Ancona harbour area, localised subsidence phenomena affecting individual buildings can be appreciated as well. There is likely no relation between these effects, probably due to soil compaction, and the landslide located SW of the city. (C) Position and ID codes of several benchmarks visited in the eight optical levelling measurement campaigns carried out in the years 1983, 1985, 1988, 1988, 1989, 1990, 1997 and 1998. All benchmarks whose estimated position is depicted on the multi-image reflectivity map have at least a PS in the immediate neighbourhood, within 100 m. (D) Optical levelling displacement data relative to benchmark 427, località Torrette (II in B), projected along the ERS Line-of-Sight. On the same plot the deformation time series relative to the closest PS is reported as well. Unfortunately, the selected PS exhibit a quite noisy behaviour ($\sigma \approx 3.5$ mm). Even though the number of levelling campaigns carried out in the 1990s is insufficient for an effective comparison, results denote good agreement. (E) Same as in (D) for benchmark 555, località Palombella, in the eastern part of the landslide ascent front area (III in B). (F) Same as in (D) for benchmark 320, località Posatora (via della Grotta) in the rural descent front area (I in B). (G) Same as in (D) for benchmark 610, località Palombella, again in the eastern part of the ascent front area (III in B). The PS time series highlights a stepwise motion (about 0.5 cm) in the time span between ERS acquisitions of 21 December 1997 and 25 January 1998, in good agreement with the displacement measured at the levelling benchmark between 1997 and 1998.

gradient near central Los Angeles in very good agreement with the estimated location and slip rate of the so-called Elysian Park blind thrust fault (Oskin et al., 2000). Further velocity field discontinuities have been identified in the area where recently the Puente Hills blind thrust was identified (Shaw and Shearer, 1999).

The comparison of PS deformation data (Table 1 and Fig. 3) with displacement time series relative to 11 GPS stations of the SCIGN (SCIGN, 2000; Heflin et al., 2000), gathering data since at least 1996 (for a reliable estimation of target velocity), highlights good agreement and allows one to appreciate the main differences. The PS technique shows up to one order of magnitude better precision than static GPS, and allows for much higher spatial sampling (hundreds of benchmarks per square kilometre, revisited every 35 days). Furthermore, the analysis of past deformation (starting from 1992) is possible exploiting the ESA ERS archive. Finally, the economic costs for wide area monitoring are much lower and no maintenance is required since PS are natural radar targets.

However, SAR displacement measurements are not 3D and the temporal resolution of GPS data from permanent stations is much higher than what currently offered by spaceborne SAR. It is worth noting that the combination of SAR data relative to both ascending and descending satellite overpasses improves significantly the results nearly doubling the PS spatial density, reducing the time interval between two passes, and allowing the retrieval of 2D displacement along both vertical and east–west directions (with different accuracy values).

The sensitivity of SAR and GPS are complementary with each other to some extent. SAR data are very sensitive to the vertical motion of the target, whereas GPS performs more poorly (Herring, 1999). On the other hand, displacement phenomena occurring approximately along the north–south direction, nearly parallel to the satellite orbit, can hardly be detected by means of SAR data only, since their projection along the ERS Line-of-Sight is very small both for ascending and descending orbits.

Moreover, SAR data accuracy, in particular the low wave number components of the velocity field, decreases slowly with the distance from the reference point. Referring to the Kolmogorov turbulence model for atmospheric artifacts (Hanssen, 1998; Williams et al., 1998; Goldstein, 1995; Ferretti et al., 1999) with

power 0.2 rad^2 1 km apart from the Ground Control Point (GCP), i.e. with heavy turbulence conditions, the accuracy of target velocity estimate with respect to the reference point is theoretically still better than 1 mm/year within ca. 16 km from the GCP (even assuming strongly unfavourable weather conditions on every acquisition day).

5. The Ancona landslide—comparison with optical levelling data

Further significant results were obtained in the framework of a PS analysis aimed at monitoring the ground deformation induced by the landslide phenomenon known as the "Grande Frana di Ancona" (Cotecchia et al., 1995; Cotecchia, 1997; Confalonieri and Mazzotti, 2001), affecting the north facing coastal slope of Montagnolo (around 2×1.75 km^2) immediately SW of the city of Ancona, Italy (Fig. 4A).

A geological description of the area in the wider context of the Umbria–Marche Apennines is available in Coteccha (1997), where geomorphology of the slope, lithology, seismicity and tectonic evolution are discussed in detail.

A major sliding event occurred on 13 December 1982, causing severe damages (Cotecchia et al., 1995; Cotecchia, 1997). Since then, a municipal monitoring program has been active. Optical levelling campaigns have been carried out in the years 1983, 1985, 1988, 1988, 1989, 1990, 1997 and 1998 highlighting vertical deformation rates in the order of a few millimeters per year. (Cotecchia et al., 1995; Cotecchia, 1997; Confalonieri and Mazzotti, 2001).

Even though the geological mechanism of the sliding phenomenon has not been clarified yet, all models take into account rotational movement features distinguishing a descent front in the inland area and an ascent front along the coast line (Confalonieri and Mazzotti, 2001). The area (in particular the descent front of the landslide, in the inland) is strongly affected by temporal decorrelation, preventing coherence from being preserved even in low normal baseline differential interferograms. Conventional DInSAR does not allow the retrieval of reliable ground deformation data.

By exploiting 61 ERS images (June 1992–December 2000), 820 PS were identified in the sliding area

and in its immediate neighbourhood (around 4×5 km^2). In particular, 12 PS are available in the rural descent front area and several dozens on both sides of the ascending front (Fig. 4). PS displacement time series have been compared with optical levelling data. Even though levelling benchmarks have been revisited too rarely for a precise description of the deformation phenomena, results are in good agreement (Fig. 4).

Again, the main properties of the two surveying techniques are complementary. Optical levelling is extremely versatile: benchmarks can be selected freely (to some extent) and the time interval between successive measurements campaigns can be fixed according to the particular displacement phenomenon at hand and, of course, the budget available. Accuracy of precise levelling is extremely high, achieving values of a fraction of millimetre 1 km apart (Inghilleri, 1974; Galloway et al., 1999).

On the other hand, high costs often prevent levelling campaigns from being performed often enough to fully characterise the deformation occurring (e.g. Ancona, Bologna (Strozzi et al., 2000), etc.). Especially for wide area monitoring, costs and spatial density of benchmarks are orders of magnitude more advantageous exploiting the PS approach. Moreover, the ERS archive allows the analysis of past deformation phenomena and, last but not least, all logistic difficulties connected to revisiting ground based benchmarks are overcome.

Particularly interesting is the possibility to gather and access all displacement data in a Geographic Information System (GIS) environment, allowing to combine interactively deformation measurements with geographical and geological data. This could facilitate reliable risk assessment and control of hazardous areas, including time/space monitoring of strain accommodation on faults, of subsiding areas and of slope instability, as well as precise stability checking of single buildings and infrastructures.

6. Conclusions

Having demonstrated the sensitivity of the method, we expect the PS analysis to play a major role whenever accurate geodetic measurements are needed (Herring, 1999), especially in urban areas, where the PS density usually ranges between 100 and 300 PS/km^2,

allowing the description of millimetric deformation phenomena with unprecedented spatial resolution.

Furthermore, the different characteristics with respect to optical levelling and GPS suggest that a synergistic use of the three techniques could improve significantly the reliability and quality of ground deformation monitoring (Colesanti et al., 2001). The PS analysis is well suited for wide area low-cost monitoring on a high-density benchmark grid. GPS provides full 3D displacement data on a low spatial density network. The versatility and vertical accuracy of optical levelling can be addressed to fully describe significant localised displacement phenomena, avoiding a huge waste of resources in planning and revisiting levelling lines far away from areas really affected by deformation.

References

Bamler, R., Hartl, P., 1998. Synthetic aperture radar interferometry. Inverse Probl., 14.

Basilico, M., 2000. Algoritmi per l'allineamento di immagini SAR

interferometriche. Tesi di Laurea in Ingegneria Elettronica. Politecnico di Milano.

California Department of Conservation, Sacramento, 1994. California Division of Mines and Geology. Fault Activity Map of California and Adjacent Areas.

Colesanti, C., Ferretti, A., Prati, C., Rocca, F., 2001. Comparing GPS, optical levelling and Permanent Scatterers. Proceedings of IGARSS 2001. Sydney, 9–13 July 2001, IEEE International, vol. 6, p. 2622–2624.

Cotecchia, V., 1997. La grande frana di Ancona. "La stabilità del suolo in Italia: zonazione sismica-frane", Atti dei Convegni Lincei, 134, Roma, 30–31 May 1996, Accademia Nazionale dei Lincei, p. 187–259.

Cotecchia, V., Grassi, D., Merenda, L., 1995. Fragilità dell'area urbana occidentale di Ancona dovuta a movimenti di massa profondi e superficiali ripetutisi nel 1982. Geol. Appl. Idrogeol. XXX (Parte I).

Confalonieri, E., Mazzotti, A., 2001. Monitoring Urban Subsidence, Cavities and Landslides by Remote Sensing (MUSCL), Technical Report WP210 "DInSAR methods and application for a coastal landslide".

Department of Oil Properties, City of Long Beach, 2000. Web site, http://www.ci.longbeach.ca.us/oil/dop/brochure.html (accessed in June 2000), recently moved to http://www.ci.long-beach.ca.us/oil/brochure.html (February 2002).

Ferretti, A., Prati, C., Rocca, F., 1999. Multibaseline InSAR DEM reconstruction: the wavelet approach. IEEE Trans. Geosci. Remote Sens. 37 (2), 705–715.

Ferretti, A., Prati, C., Rocca, F., 2000. Nonlinear subsidence rate estimation using Permanent Scatterers in differential SAR interferometry. IEEE Trans. Geosci. Remote Sens. 38 (5), 2202–2212.

Ferretti, A., Prati, C., Rocca, F., 2001. Permanent Scatterers in SAR interferometry. IEEE Trans. Geosci. Remote Sens. 39 (1), 8–20.

Fruneau, B., Achache, J., Delacourt, C., 1995. Observation and modeling of the Saint-Etienne-de-Tinée Landslide using SAR interferometry. Tectonophysics, 265.

Gabriel, K., Goldstein, R.M., Zebker, H.A., 1989. Mapping small elevation changes over large areas: differential radar interferometry. J. Geophys. Res., 94.

Galloway, D., Jones, D.R., Ingebritsen, S.E. (Eds.), 1999. Land Subsidence in the United States. Circular 1182. US Geological Survey.

Goldstein, R.M., 1995. Atmospheric limitations to repeat-track radar interferometry. Geophys. Res. Lett., 22.

Hanssen, R.F., 1998. Technical Report No. 98.1. Delft University Press, Delft.

Heflin, M., et al., 2000. http://www.sideshow.jpl.nasa.gov/mbh/series.html (data provided in May 2000).

Herring, T.A., 1999. Geodetic applications of GPS. Proc. I.E.E.E. 87 (1), 92–110.

Inghilleri, G., 1974. Topografia Generale. UTET, Torino.

Massonnet, D., Feigl, K.L., 1995. Discrimination of geophysical phenomena in satellite radar interferograms. Geophys. Res. Lett., 22.

Massonnet, D., Feigl, K.L., 1998. Radar interferometry and its application to changes in the Earth's surface. Rev. Geophys., 36.

Massonnet, D., Rossi, M., Carmona, C., Adragna, F., Peltzer, G., Feigl, K., Rabaute, T., 1993. The displacement field of the Landers earthquake mapped by radar interferometry. Nature, 364.

Massonnet, D., Feigl, K.L., Rossi, M., Adragna, F., 1994. Radar interferometric mapping of deformation in the year after the Landers earthquake. Nature, 369.

Massonnet, D., Briole, P., Arnaud, A., 1995. Deflation of Mount Etna monitored by Spaceborne Radar Interferometry. Nature, 375.

Massonnet, D., Thatcher, W., Vadon, H., 1996. Detection of post-seismic fault zone collapse following the Landers earthquake. Nature, 382.

Oskin, M., Sieh, K., Rockwell, T., Guptill, P., Miller, G., Curtis, M., Payne, M., McArdle, S., 2000. Active parasitic folds on the Elysian Park anticline: implications for seismic hazard in central Los Angeles, California. Bull. Geol. Soc. Am. 112 (5).

Peltzer, G., Rosen, P.A., Rogez, F., Hudnut, K., 1996. Postseismic rebound in fault step-overs caused by pore fluid flow. Science, 273.

Peltzer, G., Crampé, F., King, G., 1999. Evidence of the nonlinear elasticity of the crust from Mw 7.6 Manyi (Tibet) earthquake. Science, 286.

Rosen, P.A., Hensley, S., Joughin, I.R., Li, F.K., Madsen, S.N., Rodriguez, E., Goldstein, R.M., 2000. Synthetic aperture radar interferometry. Proc. I.E.E.E. 88 (3).

Sandwell, T., Price, E.J., 1998. Phase gradient approach to stacking interferograms. J. Geophys. Res., 103.

Scharroo, R., Visser, P., 1998. Precise orbit determination and gravity field improvement for the ERS satellites. J. Geophys. Res., 103.

Scripps Orbit and Permanent Array Center (SOPAC), 2000. Web site, http://www.lox.edu (accessed in May 2000), recently moved to http://www.sopac.ucsd.edu (February 2002).

Shaw, J.H., Shearer, P.M., 1999. An elusive blind-thrust fault beneath metropolitan Los Angeles. Science, 283.

Southern California Integrated GPS Network (SCIGN), 2000. Web site, http://www.scign.org/ (accessed in May 2000).

Strozzi, T., Wegmüller, U., Bitelli, G., 2000. Differential SAR interferometry for land subsidence mapping in Bologna. Proceedings of the SISOLS 2000, Rowenna, 24–29 September 2000, CNR, 187–192.

Wackernagel, H., 1998. Multivariate Geostatistics, 2nd ed. Springer-Verlag, Berlin.

Williams, S., Bock, Y., Fang, P., 1998. Integrated satellite interferometry: tropospheric noise, GPS estimates and implications for interferometric synthetic aperture radar products. J. Geophys. Res., 103.

Zebker, H.A., Villasenor, J., 1992. Decorrelation in interferometric radar echoes. IEEE Trans. Geosci. Remote Sens. 30 (5).

Zebker, H.A., Rosen, P.A., Hensley, S., 1997. Atmospheric effects in interferometric synthetic aperture radar surface deformation and topographic maps. J. Geophys. Res., 102.